

# Three-Dimensional Planar Profile Registration in 3D Scanning

João Filipe Ferreira and Jorge Dias

Institute of Systems and Robotics,  
University of Coimbra, Portugal  
{jfilipe, jorge}@isr.uc.pt

**Abstract.** Three-dimensional planar profile sampling of surfaces is a very common method of structural recovery in 3D scanning. In handheld 3D scanners, this has scarcely ever been taken into account resulting in poor precision ratings. Therefore, in this text we will describe a novel use of the profiling geometrical context to derive an intuitive and physically meaningful approach on solving the 3D profile registration problem. We will finish by describing the global optimisation algorithm and by showing experimental results achieved with a 3D scanner prototype comprising a camera, a laser-plane projector and a pose sensor.

## 1 Introduction

Most three-dimensional recovery and reconstruction systems, commonly known as 3D scanners, acquire samples of object surfaces on a three-dimensional scene so as to achieve their goal. Examples of devices resorting to this methodology are laser range finders, scanners using structured light projection, ultrasound systems, stereoscopic systems (photogrammetry), to name but a few.

Although some of these systems instantly sample complete surface patches from the object, others require a sweep of the three-dimensional scene in order to sample large sets of curvilinear profiles. More precisely, these profiles belong to planes which are projected in space in a controlled fashion in order to perform the sweep — these planes may be formed by light projection, laser projection, ultrasound projection, etc.

### 1.1 Brief Overview of Registration in 3D Scanning

Most of the research conducted regarding 3D registration has relied on the fact that large sets of points sampled from a surface from *each viewpoint* can be trusted as being accurately *locally registered* inside that set. As a result, integration can be achieved through registration of several overlapping surface patches resulting from those point-sets [1,2].

However, there is also an important group of scanners that can only trustingly yield sets of points locally registered as belonging to curvilinear planar patches. These are the main subjects of our study, and examples of these devices belong to one of the most cutting-edge and also challenging groups of 3D scanners of today: the *handheld 3D scanners*.

## 1.2 Overview of Profile Registration

There is one main difficulty regarding the 3D registration process that implies a big loss in redundancy when considering scanners that can only scan point-sets of one planar profile at a time: each profile can only be registered with other profiles that *intersect it* inside the bounds of the visible surface of the scanned object [3].

This means that it is only possible to register **crossing profiles** as opposed to overlapping surface patches and that the feature space is reduced to their intersection points. Let us assume for now that this issue has been taken care of so that intersecting profiles have been matched together. Then, one preliminary solution to the 3D registration problem for a particular profile with its set of intersecting profiles, down the line of well-known algorithms such as ICP (Iterative Closest Point), could be given by the following equation (*cf* [1,3])

$$e = \sum_{i=1}^N \left\| {}^W\mathbf{T}_{C_n} \mathbf{P}_{ni} - {}^W\mathbf{T}_{C_i} \mathbf{P}_{in}' \right\|^2, \\ \mathbf{P}_{in}' = \mathbf{P} \Big| \min_{\mathbf{P} \in p_i} \left\| {}^W\mathbf{T}_{C_n} \mathbf{P}_{ni} - {}^W\mathbf{T}_{C_i} \mathbf{P} \right\| \quad (1)$$

where  $\{C\}$  represents the local referential corresponding to the sampling sensor (usually a camera),  $\{W\}$  represents the global integrating referential and  $e$  is the error function to be minimised in a least-square sense. This function represents the sum of squares of euclidian distances between the elements of each pair, index  $i$ , of correspondent intersection points. These pairs consist of the intersection points  $\mathbf{P}_{ni}$ , taken from the considered profile  $p_n$  at point of view  $n$ , for which the transformation  ${}^W\mathbf{T}_{C_n}$  is to be estimated so as to achieve registration, and points  $\mathbf{P}_{in}'$  from the intersecting profiles  $p_i$  at point of view  $i$  (paired with transformations  ${}^W\mathbf{T}_{C_i}$ , assumed given), taken to be correspondent through matching based on the minimum euclidian distance.

Studies have been made by Hébert and Rioux, as shown in [3], that attempt to solve the local registration problem by profiting from the profiling geometry indirectly through the use of the properties of the plane which is tangent to the scanned surface so as to match points between crossing profiles.

Our solution, described in the following text, directly exploits the benefits of the profiling geometry to achieve better point correspondence, using the knowledge that intersection points between profiles also belong to the lines of intersection of crossing profile planes.

## 2 Local Optimisation for 3D Profile Registration

In the following subsections, the main contribution of our work is presented, which is twofold: a novel approach to profile matching and point correspondence, and a powerful formulation and solution of the local optimisation problem.

## 2.1 Profile Matching and Point Correspondence

In figure 1, a hypothetical (since all the true positions/orientations of all entities are assumed known) scan situation is shown, consisting of a projected plane  $\Pi_3^n$  of radiant energy<sup>1</sup> (be it light, ultrasound or of any other kind of energy propagating with a similar geometric model) crossing two other planes,  $\Pi_3^i$  and  $\Pi_3^j$ , all of which crossing an undulating surface creating profiles. Here we can clearly observe the redundancy achieved by taking advantage of its geometry, since we are considering several different entities that intersect at the same registration points: two planes, one line and two profiles for each of these points.

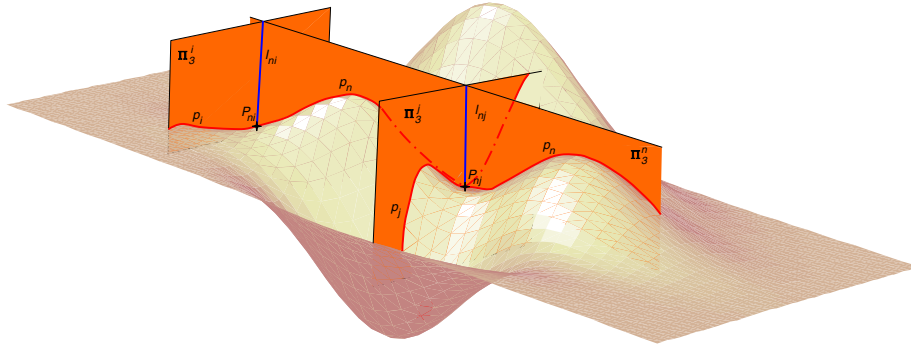


**Fig. 1.** Plane registration. One plane can be seen crossed by two other planes; their intersection lines, their corresponding profiles and the profiles' intersection points are also shown.

We propose that each light plane intersection line referred to point of view  $i$  and denoted as  $l_{in}$  can be used as a search line to determine which points belonging to profile  $p_i$  correspond to other points belonging to profile  $p_n$  in a reference point of view  $n$ .

The mathematical formalisation of 3D registration of a profile performed in this manner would thus be stated as

$$e = \sum_{i=1}^N \left\| {}^W \mathbf{T}_{C_n} \mathbf{P}_{ni} - {}^W \mathbf{T}_{C_i} \mathbf{P}'_{in} \right\|^2, \quad (2)$$

$$\begin{cases} \mathbf{P}'_{in} = l_{in} \cap p_i \\ l_{in} = {}^{C_i} \Pi_3^n \cap {}^{C_i} \Pi_3^i \end{cases}$$

where all entities have the same meanings as in equation (1), with the exception of  $\mathbf{P}'_{in}$ , which represents the correspondent point in profile  $p_i$  taken using search

<sup>1</sup> Subscript “3” appears due to the fact that the planes usually present the third restriction in triangulation based systems — see [4].

line  $l_{in}$ , which is the result of the intersection between  ${}^{C_i}\Pi_3^n$ , the plane taken from point of view  $n$ , and  ${}^{C_i}\Pi_3^i$ , the plane taken from point of view  $i$ , both referred to  $\{C_i\}$ .

## 2.2 Local Optimisation Methodology

The minimisation of the error function given by equation (2) is referred to as *local optimisation*. This particular part of the 3D registration process has been studied thoroughly in the past — it relates to the popular *absolute orientation estimation problem*, which also has applications in photogrammetry, object motion analysis, determining the hand-eye transform and pose estimation [5].

An overall study of the performances of the most popular closed-form methods proposed by several authors was done in [5]. Four major algorithms are compared in this work and it makes clear that most of them achieve similar results under realistic conditions. However, the first three methods are solutions built on top of different formulations of the *Procrustes problem* where rotation is estimated first, then translation, which for obvious reasons implies error propagation and compounding — the implications of error propagation using these types of formulations were studied in [6]. With this in mind, we have decided on using Michael Walker's solution, described in [7], which uses an elegant formulation, resorting to dual quaternions to provide a linear least-square method to solve simultaneously for rotation and translation, avoiding in this way error compounding.

According to this method, the equation that represents the transformation  $\mathbf{T}$  that takes point  $\mathbf{P}_{ni}$  into coinciding with its match  $\mathbf{P}_{in}$  is

$$\hat{\mathbf{p}}_{in} = \mathbf{W}(\hat{\mathbf{q}})^T \mathbf{Q}(\hat{\mathbf{q}}) \hat{\mathbf{p}}_{ni} + \mathbf{W}(\hat{\mathbf{q}})^T \hat{\mathbf{q}}' \quad (3)$$

where  $\hat{\mathbf{q}} = [q_1, q_2, q_3, q_4]^T$  (representing rotation) and  $\hat{\mathbf{q}}' = [q'_1, q'_2, q'_3, q'_4]^T$  (representing translation) are the real and dual parts, respectively, of the dual unit quaternion  $\hat{\mathbf{q}}$  corresponding to the screw motion related to  ${}^W\mathbf{T}_{C_n}$ , and  $\hat{\mathbf{p}}_{ni}$  and  $\hat{\mathbf{p}}_{in}$  are the purely imaginary quaternions corresponding to  $\mathbf{P}_{ni}$  and  $\mathbf{P}_{in}$ , respectively (for in-depth information regarding dual quaternions and the kinematic notion of a screw, please refer to [8]).

In addition we have the following auxiliary matrices:

$$\mathbf{K}(\hat{\mathbf{q}}) = \begin{bmatrix} 0 & -q_3 & q_2 \\ q_3 & 0 & -q_1 \\ -q_2 & q_1 & 0 \end{bmatrix}, \mathbf{Q}(\hat{\mathbf{q}}) = \begin{bmatrix} q_4 \mathbf{I} + \mathbf{K}(\hat{\mathbf{q}}) & \hat{\mathbf{q}} \\ -\hat{\mathbf{q}}^T & q_4 \end{bmatrix}, \mathbf{W}(\hat{\mathbf{q}}) = \begin{bmatrix} q_4 \mathbf{I} - \mathbf{K}(\hat{\mathbf{q}}) & \hat{\mathbf{q}} \\ -\hat{\mathbf{q}}^T & q_4 \end{bmatrix}$$

Re-writing equation (2) according to [7] and considering  $\tilde{\mathbf{p}}_{in}$ , corresponding to  $\tilde{\mathbf{P}}_{in} = {}^W\mathbf{T}_{C_i} \mathbf{P}'_{in}$ , and  $\hat{\mathbf{p}}_{in}$  resulting from equation (3), gives

$$e = \sum_{i=1}^N \beta_i \left\| \hat{\mathbf{p}}_{in} - \tilde{\mathbf{p}}_{in} \right\|^2, \quad (4)$$

$$\begin{cases} \hat{\mathbf{P}}_{in} = {}^W \mathbf{T}_{C_i} \mathbf{P}'_{in} \mapsto \tilde{\mathbf{p}}_{in} \\ \mathbf{P}'_{in} = l_{in} \cap p_i \\ l_{in} = {}^{C_i} \Pi_3^n \cap {}^{C_i} \Pi_3^i \end{cases}$$

where  $\beta_i$  are constant positive weighting factors that may be used to reflect data reliability [7,5].

Using dual quaternion properties and equation (3), one may expand the squared norm as [7]

$$\begin{aligned} \left\| \hat{\mathbf{p}}_{in} - \tilde{\mathbf{p}}_{in} \right\|^2 &= \hat{\mathbf{q}}'^T \hat{\mathbf{q}}' + 2\hat{\mathbf{q}}'^T \left( \mathbf{W}(\hat{\mathbf{p}}_{ni}) - \mathbf{Q}(\tilde{\mathbf{p}}_{in}) \right) \hat{\mathbf{q}} - 2\hat{\mathbf{q}}'^T \mathbf{Q}(\tilde{\mathbf{p}}_{in})^T \mathbf{W}(\hat{\mathbf{p}}_{ni}) \hat{\mathbf{q}} \\ &\quad + \left( (\hat{\mathbf{p}}_{ni})^T \hat{\mathbf{p}}_{ni} + (\tilde{\mathbf{p}}_{in})^T \tilde{\mathbf{p}}_{in} \right) \end{aligned} \quad (5)$$

Thus, the error function can be written as a quadratic function of  $\hat{\mathbf{q}}$  and  $\hat{\mathbf{q}}'$  [7]

$$e = \hat{\mathbf{q}}^T \mathbf{C}_1 \hat{\mathbf{q}} + \hat{\mathbf{q}}'^T \mathbf{C}_2 \hat{\mathbf{q}}' + \hat{\mathbf{q}}'^T \mathbf{C}_2 \hat{\mathbf{q}} + K \quad (6)$$

where

$$\begin{aligned} \mathbf{C}_1 &= -2 \sum_{i=1}^N \beta_i \mathbf{Q}(\tilde{\mathbf{p}}_{in})^T \mathbf{W}(\hat{\mathbf{p}}_{ni}) \\ \mathbf{C}_2 &= \left( \sum_{i=1}^N \beta_i \right) \mathbf{I} \\ \mathbf{C}_3 &= 2 \sum_{i=1}^N \beta_i \left( \mathbf{W}(\hat{\mathbf{p}}_{ni}) - \mathbf{Q}(\tilde{\mathbf{p}}_{in}) \right) \\ K &= \sum_{i=1}^N \beta_i \left( (\hat{\mathbf{p}}_{ni})^T \hat{\mathbf{p}}_{ni} + (\tilde{\mathbf{p}}_{in})^T \tilde{\mathbf{p}}_{in} \right) \end{aligned} \quad (7)$$

Using unit norm condition of the dual unit quaternion  $\check{\hat{\mathbf{q}}}$ , which in terms of its real and dual parts implies  $\hat{\mathbf{q}}^T \hat{\mathbf{q}} = 1$  and  $\hat{\mathbf{q}}'^T \hat{\mathbf{q}}' = 0$ , Walker et al. use Lagrange multipliers (see [9]) to prove that the solution for  $\hat{\mathbf{q}}$  is the eigenvector of [7]

$$\mathbf{A} = \frac{1}{2} (\mathbf{C}_3^T (\mathbf{C}_2 + \mathbf{C}_2^T)^{-1} \mathbf{C}_3 - \mathbf{C}_1 - \mathbf{C}_1^T) \quad (8)$$

corresponding to its largest positive eigenvalue. The solution for the dual part is easily shown to be  $\hat{\mathbf{q}}' = -(\mathbf{C}_2 + \mathbf{C}_2^T)^{-1} \mathbf{C}_3 \hat{\mathbf{q}}$  [7].

### 3 The 3D Planar Profile Registration Algorithm

The global algorithm for three-dimensional profile registration can be described as the successive iteration of the steps described in the text that follows, using prior knowledge of the approximate attitude of each radiant energy plane (as said in section 2.1, this can be light, ultrasound, etc.) as an initial value source for transformation estimates.

At iteration  $t$  all  $\mathbf{T}_n(t)$ ,  $n = 1..m$  for a total of  $m$  profiles are estimated as follows:

1. Firstly, sets of all other energy planes which are known to cross each referential energy plane inside surface bounds are grouped. Planes which are not intersected may be eliminated as lacking information, if wanted.
2. Next, each set of intersecting planes is processed by reference plane, and points belonging both to the reference plane and to each corresponding crossing plane which are closest to the intersection line estimates are determined and matched per intersection line. Correspondences are validated if distances between matched points are lower than a threshold.
3. Equation (4) is solved as described earlier so as to determine  $\mathbf{T}_n(t)$ . To this end, transformations  ${}^W\mathbf{T}_{C_i}$  corresponding to iteration  $t - 1$  are used. The weights  $\beta_i$  are computed resorting to two unit and scale independent measures: the so-called *Tanimoto measure or distance* (similarity or proximity measure) between two 3D points  $\mathbf{x}$  and  $\mathbf{y}$  given by [10,11]

$$S_T(\mathbf{x}, \mathbf{y}) = \frac{\mathbf{x}^T \mathbf{y}}{\|\mathbf{x}\|^2 + \|\mathbf{y}\|^2 - \mathbf{x}^T \mathbf{y}} = \frac{1}{1 + \frac{(\mathbf{x}-\mathbf{y})^T (\mathbf{x}-\mathbf{y})}{\mathbf{x}^T \mathbf{y}}} \quad (9)$$

which is noticeably inversely proportional to the squared euclidean distance between the points divided by its correlation, and is thus normalised; the normalised orthogonality, measure between two crossing planes (i.e. crossing planes which are “more” orthogonal yield more important correspondences) with normals  $\hat{\mathbf{n}}$  and  $\hat{\mathbf{m}}$ , respectively, given by

$$O(\hat{\mathbf{n}}, \hat{\mathbf{m}}) = 1 - \hat{\mathbf{n}} \cdot \hat{\mathbf{m}} \quad (10)$$

Hence,  $\beta_i = S_T^j \cdot O^k$ , was used, where  $j$  and  $k$  may be chosen empirically, given the characteristics and average performance ratings of the scanner.

4. Finally, the global correspondence error given by the sum of distances between points is computed — if less than a chosen error threshold, the algorithm is considered as having converged and is stopped; otherwise, the algorithm proceeds to the next iteration. Another stopping condition is met if all  $\mathbf{T}_n(t)$  approximate the identity matrix.

### 4 Results and Discussion

Figure 2 on the next page shows the handheld 3D laser scanner prototype which was used to scan a mannequin for the experimental application of the 3D planar

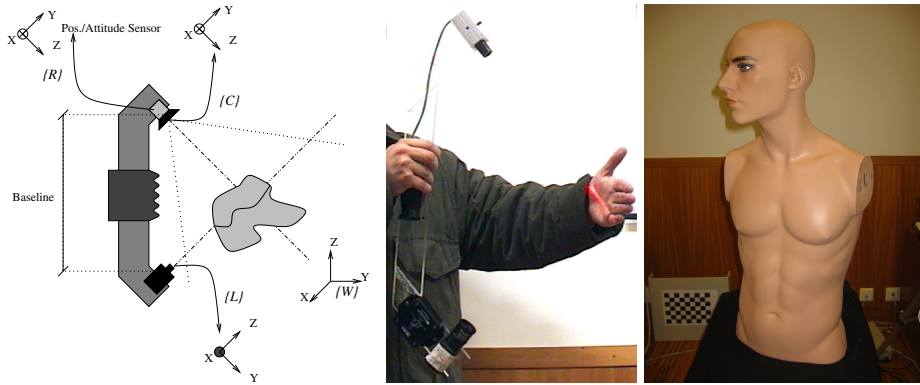


**Fig. 2.** The Tele-3D handheld scanner’s schematics and photo on the left and the mannequin test subject on the right. The Tele-3D is a triangulation-based laser scanner with a camera, a laser-plane projector and a pose sensor mounted on a boomerang-shaped acrylic structure.

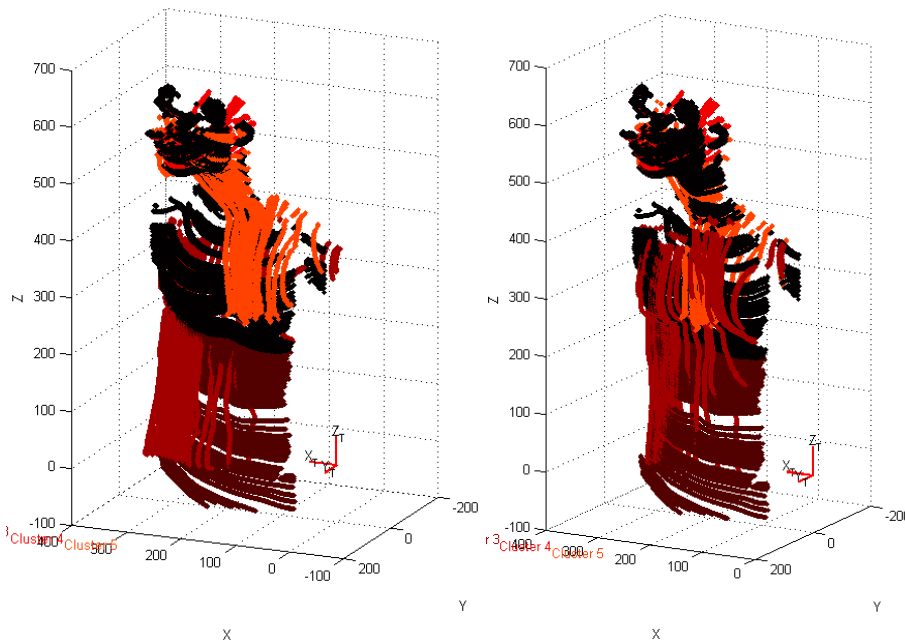


**Fig. 3.** 3D planar profile registration — on the left, pre-integration using the pose sensor readings to obtain initial values for transformations is shown; on the right, the final result using our method is presented. Profiles with clearly different orientations were clustered and represented with different colours so as to improve visualisation of the results.

profile registration algorithm. This system was set up using proprietary calibration algorithms<sup>2</sup>, which produced estimates for triangulation errors per profile of 2.6 mm and for pose orientation and position readings of 2.7° and 12.6 mm, respectively [4]. Considering the magnitude of these error estimates, especially the latter, good performance for the registration algorithm was paramount.

On figure 3 on the preceding page, the results yielded before (using the pose sensor readings to obtain initial values for transformations) and after the registration/integration process are shown [4]. The success of the proposed registration algorithm can be clearly seen by the reasonable re-orientation of the profiles yielded with its application.

## References

1. Chen, Y., Medioni, G.: Object Modelling by Registration of Multiple Range Images. *Image and Vision Computing* **10** (1992) 145–155
2. Rusinkiewicz, S., Levoy, M.: Efficient variants of the ICP algorithm. In: *Proceedings of the Third Intl. Conf. on 3D Digital Imaging and Modeling*. (2001) 145–152
3. Hébert, P., Rioux, M.: Toward a hand-held laser range scanner: Integrating observation-based motion compensation. In: *Proceedings of IS&T/SPIE's 10th Annual Symposium on Electronic Imaging (Photonics West); Conference 3313: Three-Dimensional Image Capture and Applications*, San Jose, Ca, USA (1998)
4. Ferreira, J.: *Tele-3d: Um scanner para registo tridimensional de objectos*. Master's thesis, Department of Electrical Engineering and Computer Science, University of Coimbra, Portugal (2004)
5. Eggert, D.W., Lorusso, A., Fisher, R.B.: Estimating 3-D rigid body transformations: a comparison of four major algorithms. *Machine Vision and Applications* (1997) 272–290
6. Dorst, L.: First order error propagation of the procrustes method for 3-d attitude estimation. In: *IEEE Transactions on Pattern Analysis and Machine Intelligence*. Volume 27. (2005) 221–229
7. Walker, M.W., Shao, L., Volz, R.A.: Estimating 3-D Location Parameters Using Dual Number Quaternions. *CVGIP: Image Understanding* **54** (1991) 358–367
8. Daniilidis, K.: Hand-Eye Calibration Using Dual Quaternions. *International Journal of Robotics Research* (1998)
9. Rao, S.S.: 12. In: *Applied Numerical Methods for Engineers and Scientists*. Prentice Hall (2002) 899–902 Sections 12.4.3/12.4.4 — Function of Several Variables with Equality Constraints/Mixed Equality and Inequality Constraints.
10. Tanimoto, T.T.: An elementary mathematical. Technical report, IBM (1959) As cited by [11].
11. Scott, S., Cao, L.: *Topic clustering basic* (1999) CSCE 970: Pattern Recognition Spring Semester.

---

<sup>2</sup> For more details concerning the Tele-3D scanner and its calibration algorithms, please refer to [4] and <http://paloma.isr.uc.pt/www/Tele3DWeb>.